J Supercond Nov Magn (2017) 31:873–878
DOI 10.1007/s10948-017-4240-0

ORIGINAL PAPER

Switching of Coercivity Process in MnBi Alloys

J. Zamora[1] · I. Betancourt[1] · I. A. Figueroa[1]

Received: 23 June 2017 / Accepted: 28 June 2017 / Published online: 4 August 2017

Abstract MnBi-based alloys represent an interesting choice for developing rare earth-free permanent magnets due to the high magnetocrystalline anisotropy of their characteristic low-temperature intermetallic phase (LTIP) with hexagonal structure. In this work, we discuss the switching of coercivity mechanism in MnBi alloys by modulation of their phase distribution and microstructure. As-cast MnBi alloys obtained by suction-casting technique exhibited LTIP interspersed within Bi- and Mn-rich areas. A noticeable coercivity field of 282 kA/m was observed. The coercivity mechanism for this alloy was explained in terms of the nucleation of reverse domains after saturation, by means of the Kronmüller equation, which incorporates the detrimental effect of microstructure defects through fitting parameters associated to reduced intrinsic magnetic properties at grain size boundaries, interfaces, and local demagnetizing fields. Subsequent annealing at 583 K for 24 h produced a marked reduction of coercivity (down to 16 kA/m), reflecting a switching of coercivity process from nucleation to pinning of domain walls. The key microstructural feature determining this variation is the formation/suppression of Bi-rich areas, which promotes the nucleation and growth of the initial MnBi intermetallic phase.

Keywords Hard magnetic properties · High coercivity · Permanent magnets

✉ I. Betancourt
israelb@unam.mx

[1] Departamento de Materiales Metálicos y Cerámicos, Instituto de Investigaciones en Materiales, Universidad Nacional Autónoma de México, 04510 D.F. Mexico, Mexico

1 Introduction

The search for new permanent magnets with rare earth-free compositions has elicited a renewed interest due to the possibility for obtaining high-performance magnets at competitive cost relative to the well-known neodymium-iron-boron supermagnets. In particular, MnBi-based alloys represent an interesting option for developing permanent magnets due to their characteristic low-temperature intermetallic phase (LTIP) possessing ferromagnetic ordering with Curie temperature around 620 K and an NiAs-type hexagonal structure with spatial group $P6_3/mmc$. LTIP presents an attractive uniaxial magnetocrystalline anisotropy characterized by an anisotropy constant (K_1) of 0.90×10^6 J/m^3 and a saturation magnetization ($\mu_0 M_s$) of 0.73 T, which compares very well with other types of hard magnetic materials, such as hard ferrites and rare earth-iron-boron alloys with off-stoichiometric compositions [1, 2]. In addition, MnBi alloys have positive temperature coefficient of coercivity [3–6], which renders these alloys as suitable magnetic materials to obtain permanent magnets able to operate at high temperatures, and hence, with great potential for a variety of applications including wind turbine, electric vehicle, magnetic transmission machines, and microelectro-mechanical systems [7]. Unfortunately, obtaining a single-phase LTIP-MnBi alloy is difficult, because its formation occurs through a peritectic reaction, and thus, the formation of secondary phases is not easy to avoid, according to the phase diagram shown in Fig. 1 [8].

Thermodynamically, at the peritectic point, the transforming phases, i.e., liquid and Mn, will form the Mn–Bi phase. As the diffusion process for this alloy is extremely slow (at low temperatures) [9], the full formation of such intermetallic phase is normally not achieved, that is why the

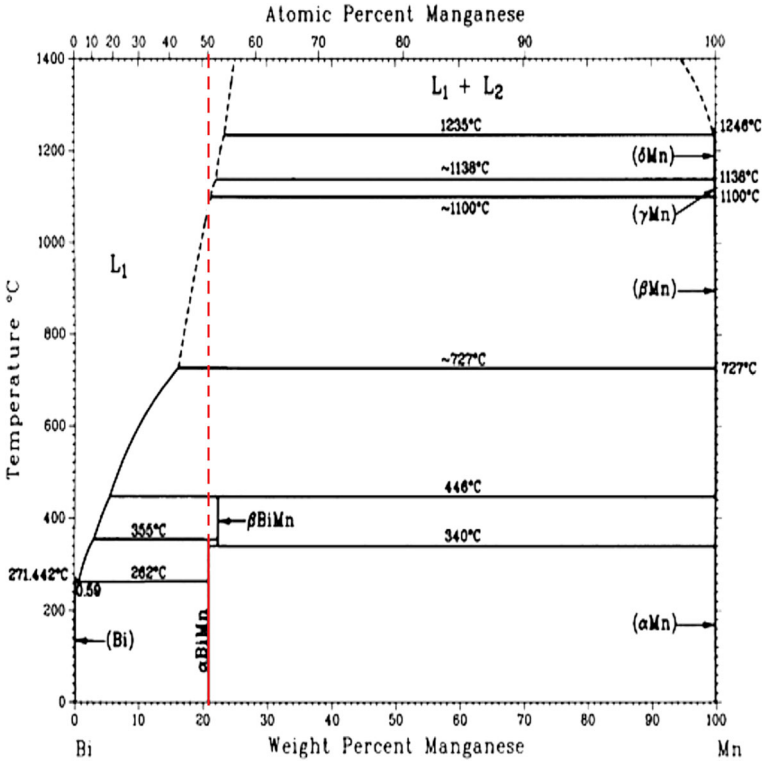

Fig. 1 Phase diagram for Mn–Bi alloy system. The line in *red* indicates the peritectic formation of the LTIP MnBi (adapted from [8])

Mn or Bi phases are normally observed within the structure. Nevertheless, it has been reported that the formation of the LTIP is feasible by rapid cooling from liquid temperature to below 628 K [10]. Above this temperature, a structural transition occurs from NiAs type to a distorted hexagonal Ni_2In type, changing the magnetic phase transition to a high paramagnetic temperature phase (HTP) [10, 11]. However, the first peritectic decomposition is located at 628 K, $MnBi \rightarrow Mn_{1.08}Bi$ + Bi-rich liquid and a subsequent phase decomposition takes place at 719 K, according to the following reaction: $Mn_{1.08}Bi \rightarrow Mn$ + Bi-rich liquid [11, 12]. Additionally, there is a eutectic reaction at 535 K, $L \rightarrow Bi + \alpha MnBi$, which causes a decrease in the operating temperature. When the HTP is rapidly cooled, a metastable state identified as ferromagnetic high-temperature phase (QHTP) with a Curie temperature of 440 K is obtained [12]. Several methods have been reported for obtaining the LTIP, such as arc melting, powder metallurgy, melt spinning, and induction furnace [10, 13–20], for which coercivity values within the range 4.0–955 kA/m were attained, together with saturation magnetization variation between 0.1 and 0.7 T. For these methods, a subsequent heat treatment is required to achieve a complete phase formation [1]. On the other hand, in ref. [21], it is reported a different preparation approach based on metal-redox method to synthesize single-domain MnBi nanoparticles stable in air, with average size below 300 nm, for which remarkable coercive fields as high as 1193 kA/m were achieved, together with saturation magnetization of 0.48 T.

An important aspect for developing high-performance permanent magnets is the proper understanding of the coercivity mechanism governing the magnetic hardening of the material. In this sense, the main approaches for describing the coercivity (H_c) of magnetic materials are the nucleation-controlled process and pinning of magnetic domain walls. For the first case, the development of high H_c values relies on the nucleation field H_N necessary for the onset of magnetization reversal, which occurs at the interface of non-magnetic grains, defects, or significant misalignment between magnetic grains [22]. On the other hand, pinning of magnetic domain walls depends on the size and morphology of the phases present within the material's microstructure. The critical length L_{crit} for the formation of magnetic domains is given by [22] the following:

$$L_{crit} = \frac{72}{\mu_0 M_s^2}\sqrt{AK_1} \tag{1}$$

where A corresponds to the exchange constant of the material. If the magnetic phase has a characteristic length $L > L_{crit}$, magnetic domains will appear as part of the magnetic structure in order to decrease the overall magnetostatic energy of the material. The concomitant formation of magnetic domain walls will promote a coercivity mechanism by means of their pinning at the defects of the materials' microstructure, such as inclusions, secondary non-magnetic phases, vacancies, grain boundaries or interfaces, for which the intrinsic magnetic properties (such as K_1, A, or M_s) are usually reduced or even vanished.

In this work, we report and discuss the phase constitution and its influence on the coercivity mechanism of MnBi alloys obtained by a suction casting technique, a preparation route not reported yet for this type of alloys.

2 Experimental Techniques

Initial ingots of Bi–Mn master alloy were obtained by means of arc melting of elemental constituents in a titanium-gettered inert atmosphere. The samples were remelted at least five times to ensure chemical uniformity. From the master ingots, cylindrical rods were prepared by the suction casting technique with the following dimensions: 3-mm diameter and a length of 30 mm. After that, the cylindrical rods were annealed at 583 K for 24 h in argon-filled sealed quartz tubes and subsequently quenched in water. Phase distribution was determined by x-ray diffraction (XRD) using a Siemens D5000 diffractometer with Co–Ka radiation ($\lambda = 1.7903$). Microstructural analysis was performed by a field-emission scanning electron microscopy (SEM) in a JEOL 7600F equipment. Magnetic measurements were carried out by using a vibrating sample magnetometer (VSM) LDJ 9600 with a maximum applied field of 1193 kA/m. Curie temperature was determined by using magnetic thermogravimetric analysis (MTGA) in a TA Q500 thermobalance with a heating rate of 10 K/min, coupled with a permanent magnet.

3 Results

3.1 Phase Distribution Analysis and Microstructure

Figure 2a shows the XRD pattern corresponding to the as-cast alloy obtained by suction casting. The diffractogram revealed the presence of elementary Bi, Mn, and the LTIP-MnBi, according to the ICDD files [00-044-1246], [01-089-2412], and [03-065-8733], respectively. From the main peaks, the experimental unit cell parameters for the LTIP-MnBi were determined as $a = 4.305$ Å and $c = 6.128$ Å, yielding a unit cell volume $V = 98.37$ Å^3. These results are consistent with those reported in the ICDD PDF #03-065-8733 ($a = 4.305$ Å, $c = 6.118$ Å, and $V = 98.19$ Å^3). The precipitation of the secondary phases can be attributed to the fact that, during the cooling process, Bi tends to nucleate from sub-cooled liquid before the formation of the peritectic phase LTIP-MnBi [16, 17], whereas the segregation of Mn is favored by the presence of Mn–Bi + liquid area during the peritectic reaction. The presence of secondary phases such as elemental Bi and Mn has been also reported in others works such as in [17, 23, 24].

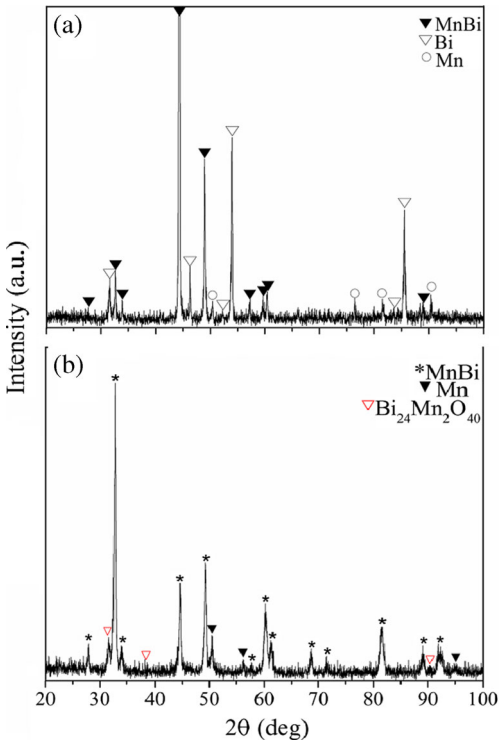

Fig. 2 XRD pattern for **a** as-cast MnBi alloy and **b** MnBi alloy annealed at 583 K for 24 h

Figure 2b shows the XRD pattern of the alloy after the heat treatment at 583 K for 24 h. This figure clearly shows that all the diffraction peaks of segregated Bi disappeared and that LTIP-MnBi phase remains as the main structural component of the heat-treated alloy. Minor secondary (Bi, Mn)-oxide phase was also identified, which reflects the susceptibility of the LTIP-MnBi to oxygen presence. After heat treatment, the amount of the intermetallic MnBi phase increased due to the mixing of the remaining Bi atoms with Mn to form LTIP. Nevertheless, once the Bi was depleted, the remaining portion of pure Mn was heterogeneously segregated in the form of α-Mn.

Figure 3 exhibits an SEM micrograph for the MnBi as-cast alloy. Within this figure, three regions are clearly visible (Fig. 3a): black zones dispersed over a dominant light gray region, together with dark gray areas. Energy-dispersive spectroscopy (EDS) composition analysis showed that such regions corresponded to pure Mn, pure Bi, and to the LTIP-MnBi, respectively (Fig. 3b). This MnBi phase is observed throughout the sample with undissolved Mn particles embedded in a diamagnetic Bi-rich matrix. Clearly, the cooling rate of the suction-casting process is not fast enough to prevent Mn from precipitating as segregated phase. The MnBi areas showed variable sizes, i.e., with lengths between 2.0 and 6.0 µm, whereas the Mn and Bi zones displayed lengths between 5.0 and 3.0 µm, respectively. Few inclusions with darkest contrast within Mn zones

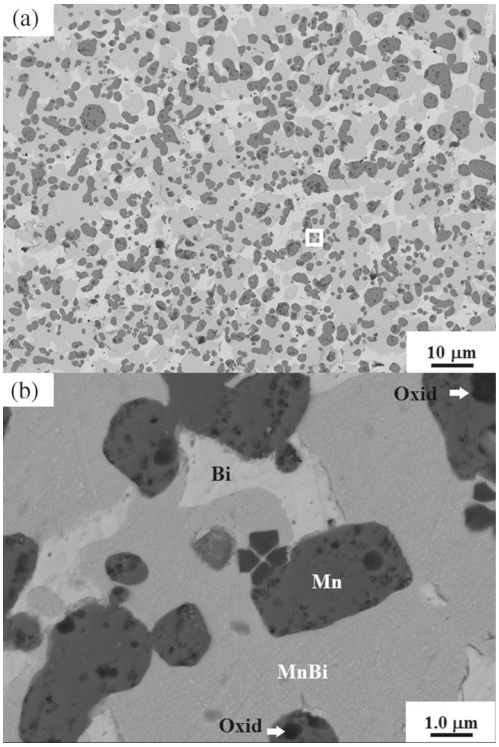

Fig. 3 **a** SEM micrographs for the as-cast MnBi alloy obtained by suction-casting technique showing LTIP-MnBi zones together with the segregated Mn and Bi phases. **b** Amplified image from the *highlighted white square*

(Fig. 3b) correspond to the (Mn, Bi)-oxide. According to the phase diagram (Fig. 1), the Mn is in a liquid phase for temperatures above 1373 K and, for cooling below the eutectic temperature 565 K, the alloy will contain a minor amount of segregated Bi promoting the formation of LTIP-MnBi. However, as the MnBi melt begins to cool down from the liquid to the peritectic temperature 628 K, the segregation of Mn occurs concomitantly, which in turn favors its precipitation together with Bi and MnBi intermetallic phases. Once the peritectic temperature is reached, the MnBi phase begins to solidify surrounded by the Bi-rich phase.

In contrast, the microstructure of the annealed sample (Fig. 4) indicated that pure Bi zones were suppressed, whereas numerous round-like grains of manganese are still present, having an average length of 1.41 ± 0.6 μm, embedded within a majority LTIP-MnBi areas. Annealing temperature below 613 K promotes the diffusion of more Mn atoms into bismuth lattice sites and hence, facilitating the precipitation of MnBi phase [25]. Such MnBi areas exhibited a noticeable growth, with uniformly distributed lengths ranging from 30 to 50 μm, as observed in Fig. 4. Some few (Bi, Mn)-oxide areas were also identified, which are also consistent with the XRD analysis. The formation of oxide phases can be attributed to a small amount of remaining oxygen

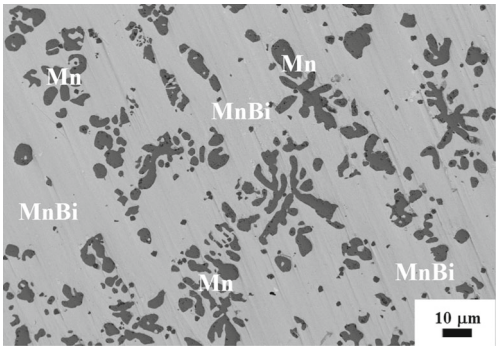

Fig. 4 SEM micrograph for the MnBi alloy annealed alloy at 583 K for 24 h. LTIP is the predominant phase. A reduced amount of round-like grains of Mn phase (with an average grain size of 1.41 ± 0.6 μm) is observed embedded within MnBi matrix

within the casting chamber, which can react with the Mn and Bi atoms during annealing.

3.2 Magnetic Properties

Second quadrant of the hysteresis curve (demagnetizing section) measured at room temperature for the MnBi as-cast alloy is shown in Fig 5a. This sample exhibited hard magnetic behavior characterized by a noticeable coercive field (H_c) of 282 kA/m and a remanence magnetization of 0.01 T. Saturation magnetization ($\mu_0 M_s$) was of 0.03 T. The coercive field, being an extrinsic magnetic property, depends markedly on microstructural features (grain size, point defects, grain boundaries, inclusions, internal stresses, non-magnetic phases) as well as intrinsic properties such as magnetocrystalline anisotropy [22]. The presence of non-magnetic Bi-rich zones interspersed between the magnetic MnBi phase causes a dilution effect on the magnetic moment of the alloy sample, leading to the rather low $\mu_0 M_s$ observed. Figure 5b exhibits the coercivity H_c as a function of temperature T within the interval 200–360 K, for which the characteristic increasing behavior (magnetic hardening) with increasing temperature of the LTIP is manifested. Figure 5c displays the thermogravimetric (MTGA) curve showing the weight variation ΔW as a function of temperature for same alloy. The step-like form of the plot is indicative of the magnetic order-disorder transition at the Curie temperature, T_c, which was located at 617 K. This T_c value is consistent with the reported transition of the LTIP [2, 7].

Within the frame of the nucleation-controlled mechanism for coercivity, it is possible to explain the development of high H_c values in terms of the nucleation field H_N necessary for the onset of magnetization reversal, which occurs at the interface of non-magnetic grains, defects, or significant misalignment between magnetic grains. For our as-cast MnBi alloys, the onset of magnetization occurs at the interface

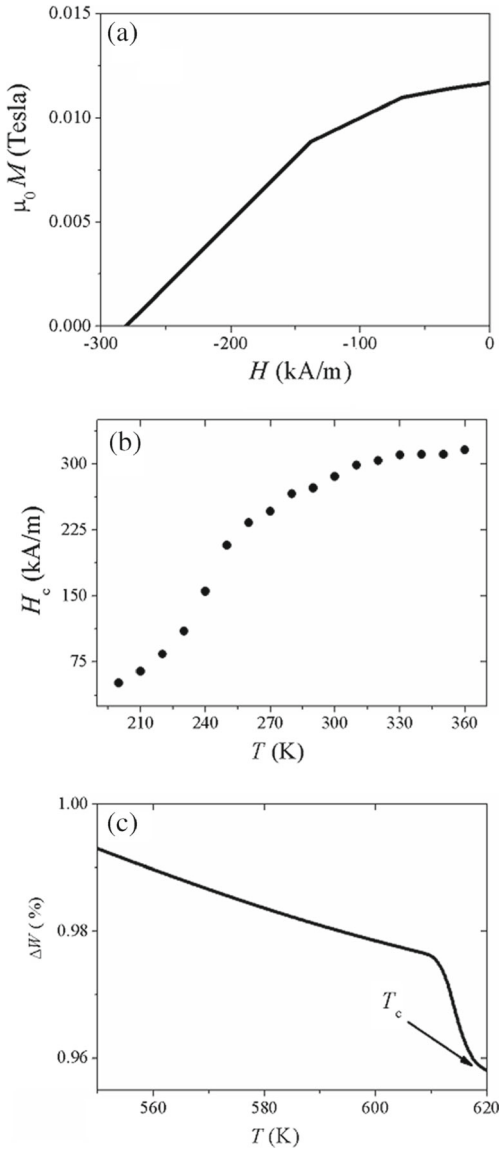

Fig. 5 Magnetic properties for the as-cast MnBi alloy obtained by suction-casting: **a** demagnetizing *M–H* curve, **b** Coercivity field H_c as a function of temperature, **c** MTGA curve showing Curie transition at 617 K

between magnetic LTIP phase and non-magnetic Bi surrounding areas since, at such interfaces, the reduction of the magnetocrystalline constant K_1 facilitates the nucleation of reversed domains. According to Kronmüller and Fähnle [22], in order to incorporate the detrimental influence of microstructural defects in real materials (point defects, grain boundaries, non-magnetic phases) the proper equation for H_c is given by

$$H_c = H_N^{\min}\alpha_K - N_{\text{eff}}(\mu_0 M_s) \tag{2}$$

where $H_N^{\min}$ represents the minimum nucleation field ($H_N^{\min} = K_1/M_s$), α_K is a microstructural parameter representing the reduction of K_1 at the surface interfaces with non-magnetic regions, and N_{eff} is an average effective demagnetization factor describing the internal stray fields acting on the grains. This equation for coercivity has been proved successfully in sintered Nd–Fe–B-based magnets [26, 27], whose microstructural characteristics are equivalent to our as-cast MnBi alloys. Since both α_K and N_{eff} parameters are non-temperature-dependent, it is feasible to use them as fitting factors in (2). Taking into account that the reported variation of α_K and N_{eff} parameters for hard magnetic alloys with equivalent microstructure is between 0.89–0.93 and 1.0–5.0, respectively [27], we use $\alpha_K = 0.91$ and $N_{\text{eff}} = 1.45$ to obtain $H_c = 279$ kA/m, which is very close to the experimental result for our as-cast MnBi alloy. Kronmüller equation also sheds light on the increasing behavior of H_c, since K_1 rapidly increases with increasing temperature [2, 28], which in turn determines a growing $H_N^{\min}(T)$ response and hence, an augmenting H_c with rising temperature.

Subsequent annealing of the as-cast alloy produced a marked decrease for H_c (down to 16 kA/m), alongside a noticeable enhancement of $\mu_0 M_s$ (up to 0.47 T), as illustrated in Fig. 6 by the corresponding *M–H* curve. The increment of M_s can be ascribed to the significant rise of the volume fraction of ferromagnetic LTIP.

This adjustment of magnetic properties is indicative of a significant change of coercivity mechanism causing a magnetic softening of the alloy. Specifically, the reduction of H_c can be attributed to the formation of extensive ferromagnetic LTIP areas (with typical lengths varying between 30 and 50 μm, see Fig. 4), favoring the formation of magnetic domain walls, which in turn, switches the coercivity mechanism from nucleation to pinning process, and hence, to lower H_c values. The formation of magnetic domains for MnBi structures with lengths $L^{\text{MnBi}} > 30$ μm is feasible since its critical length (given by (1)) is $L_{\text{crit}}^{\text{MnBi}} = 0.864$ μm (considering the exchange constant of MnBi alloys as $A = 2.86 \times 10^{-11}$ J/m [22]), which clearly implies $L^{\text{MnBi}} \gg$

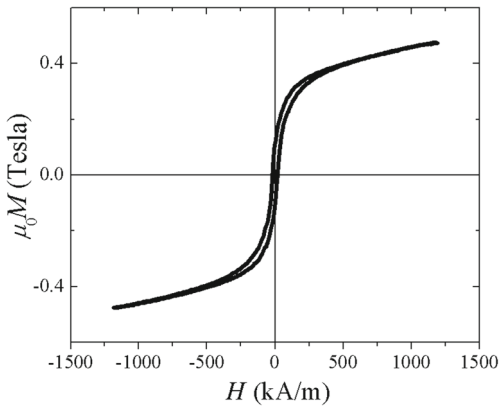

Fig. 6 *M–H* curve for the annealed MnBi alloy at 583 K for 24 h

L_{crit}^{MnBi}. Upon the formation of magnetic domains, the remaining Mn grains act as inclusions promoting the pinning of the domain walls. For pinning mechanism, the propagation field H_p associated to the coercivity of the material can be calculated as follows [29]:

$$H_p = \frac{\gamma_w}{\mu_0 M_s R_0} \tag{3}$$

where γ_w stands for the energy of the domain wall and R_0 corresponds to the radius of the inclusion. By using $\gamma_w = 4\sqrt{AK_1} = 2.03 \times 10^{-2}$ J/m^2 and $R_0 = 1.41$ μm (corresponding to the average value of the Mn grains of 1.41 μm ± 0.6), we obtain $H_p = H_c = 19.7$ kA/m, which is very close to the experimental coercivity observed for our annealed MnBi alloy.

4 Conclusions

The coercivity mechanism of MnBi alloys can be modulated by phase constitution and microstructural features, in particular, through the formation/suppression of Bi-rich zones surrounding the ferromagnetic LTIP, which in turn determines the alloy coercivity variation from 282 to 16 kA/m. The coercivity mechanism switched from nucleation controlled magnetization reversal mode for the as-cast alloy, to pinning process promoted by the formation Mn-based inclusions embedded within extensive LTIP areas.

Acknowledgments I. Betancourt acknowledges financial support from research project UNAM-PAPIIT IN103216. J. Zamora is grateful for the scholarship received from UNAM-PAPIIT IN103216 and CONACyT-Mexico. Special thanks are given to Adriana Tejeda and Josue Romero (IIM-UNAM) for their valuable technical assistance.

References

1. Guo, X., Chen, X., Altounian, Z., Strom-Olsen, J.O.: Magnetic properties of MnBi prepared by rapid solidification. Phys. Rev. B **46**, 14578–14582 (1992)
2. Chen, T., Sturius, W.R.: The phase transformation and physical properties of the MnBi and Mn1.08Bi compounds. IEEE. Trans. Magn. **10**, 581–586 (1974)
3. Williams, H.J., Sherwood, R.C., Boothby, O.L.: Magnetostriction and magnetic anisotropy of MnBi. J. Appl. Phys. **28**, 445–447 (1957)
4. Guo, X., Chen, X., Altounian, Z., Olsen, J.O.S.: Temperature dependence of coercivity in MnBi. J. Appl. Phys. **73**, 6275–6277 (1993)
5. Ping Liu, J., Fullerton, E., Gutfleishch, O., Sellmyer, D.J. Nanoscale Magnetic Materials and Applications, 1st edn. Springer, US (2009)
6. Liu, Y., Sellmyer, D.J. Shindo: Handbook of Advanced Magnetic Materials, 1st edn., vol. 1. Springer, US (2006)
7. Coey, J.M.D.: Hard magnetic materials: perspective. IEEE Trans. Magn. **47**, 4671–4681 (2011)
8. Okamoto, H.: Bi-mn phase diagram. Alloy phase diagrams. Materials Park OH: ASM International (1990)
9. Andresen, A.F.: The magnetic and crystallographic properties of MnBi studied by neutron diffraction. Acta. Chem. Scand. **21**, 1543–1554 (1967)
10. Nithya, R., Singh, N., Singh, S.K., Gahtori, B., Mishra, S.K., Dhar, A., Awana, V.P.S.: Appreciable magnetic moment and energy density in single-step normal route synthesized MnBi. J. Supercond. Nov. Magn. **26**, 3161–3165 (2013)
11. Yin, F., Gu, N.: Sintering formation of low temperature phase MnBi and its disordering in mechanical milling. J. Mater. Sci. Technol. **12**, 335–341 (1996)
12. Koyama, K., Onogi, T., Mitsui, Y., Nakamori, Y., Orim, S., Watanabe, K.: Magnetic phase transition of MnBi under high magnetic fields and high temperature. Mater. Trans. **48**, 2414–2418 (2007)
13. Kharel, P., Skomski, R., Kirby, R.D., Sellmyer, D.J.: Structural, magnetic and magneto-transport properties of Pt-alloyed MnBi thin films. J. Appl. Phys. **107**, 09E303 (2010)
14. Yoshida, H., Shima, T., Takahashi, T., Fujimori, H.: Preparation of highly pure MnBi intermetallic compounds by arc-melting. Mater. Trans. JIM **40**, 455–458 (1999)
15. Isogai, K., Matsuura, M., Tezuca, N., Sugimoto, S.: Magnetic properties of MnBi fine particles fabricated using hydrogen plasma metal reaction. Mater. Trans. JIM **54**, 1673–1677 (2013)
16. Saito, T., Nishimura, R., Nishio-Hamane, D.: Magnetic properties of Mn-Bi melt-spun ribbons. J. Magn. Magn. Mater. **349**, 9–14 (2014)
17. Zhang, D.T., Cao, S., Yue, M., Liu, W.Q., Zhang, J.X., Qiang, Y.: Structural and magnetic properties of bulk MnBi permanent magnets. J. Appl. Phys. **109**, 07A722 (2011)
18. Zhang, D.T., Geng, W.T., Yue, M., Liu, W.Q., Zhang, J.X., Sundararajan, J.A., Qiang, Y.: Crystal structure and magnetic properties of Mn_xBi_{100-x}(x = 48, 50, 55 and 60) compounds. J. Magn. Magn. Mater. **324**, 1887–1890 (2012)
19. Nguyen, P.K., Jin, S., Berkowitz, A.E.: Unexpected magnetic domain behavior in LTP-mnbi. IEEE Trans. Magn. **49**, 3387–3390 (2013)
20. Nguyen, P.K., Jin, S., Berkowitz, A.E.: Mnbi particles with high energy density made by spark erosion. J. Appl. Phys. **115**, 17A756 (2014)
21. Kirkeminde, A., Shen, J., Gong, M., Cui, J., Ren, S.: Metal-redox synthesis of MnBi hard magnetic nanoparticles. Chem. Mater. **27**, 4677–4681 (2015)
22. Kronmüller, H., Fähnle, M.: Micromagnetism and the Microstructure of Ferromagnetic Solids. Cambridge University Press, Cambridge (2003)
23. Kavita, S., Seelam, U.M.R., Prabhu, D., Gopalan, R.: On the temperature dependent magnetic properties of as-spun Mn-Bi ribbons. J. Magn. Magn. Mater. **377**, 485–489 (2015)
24. Basso, V., Olivetti, E.S., Martino, L., Küpferling, M.: Entropy change and kinetic effects at the magnetostructural phase transition of MnBi. Int. J. Refrig. **37**, 266–272 (2014)
25. Unger, W.K., Slotz, M.: Growth of MnBi films on mica. J. Appl. Phys. **42**, 1085–1089 (1971)
26. Kronmüller, H.: Micromagnetic background in hard magnetic materials. In: Long, G.J., Grandjean, F. (eds.) Supermagnets, hard magnetic materials, p. 461. Kluwer, Dordrecht (1991)
27. Kou, X.C., Kronmüller, H., Givord, D., Rossignol, M.F.: Coecivity of sintered $Pr_{17}Fe_{75}B_8$ and $Pr_{17}Fe_{53}B_{30}$ permanent magnets. Phys. Rev. B **50**, 3849 (1994)
28. Curcio, C., Olivetti, E.S., Martino, L., Kupferling, M., Basso, V.: Study of the temperature dependence of coercivity in MnBi. Phys. Procedia **75**, 1230–2137 (2015)
29. Skomski, R., Coey, J.M.D.: Permanent Magnetism. Institute of Physics, London (1999)